Eur. Phys. J. B **29**, 533–540 (2002)
DOI: 10.1140/epjb/e2002-00336-1

THE EUROPEAN PHYSICAL JOURNAL B

A lower bound for the volume-averaged mean-square magnetostatic stray field

A. Michels[1,2,a], J. Weissmüller[1,2], and R. Birringer[2]

[1] Institut für Nanotechnologie, Forschungszentrum Karlsruhe, Karlsruhe, Germany
[2] Technische Physik, Universität des Saarlandes, Saarbrücken, Germany

Received 25 April 2002
Published online 31 October 2002 –

Abstract. Based on a micromagnetics model, we develop a method through which quantitative information on the volume-averaged mean-square magnetostatic stray field $\langle|\mathbf{H}_d^b|^2\rangle_v$ due to non-zero divergences of the magnetization $\mathbf{M}$ within the bulk of a ferromagnetic body can be obtained by analysis of magnetic-field-dependent small-angle neutron scattering data. In the limit of high applied magnetic field $\mathbf{H}_a$, when the direction of $\mathbf{M}$ deviates only sligthly from $\mathbf{H}_a$, we have estimated a lower bound for $\langle|\mathbf{H}_d^b|^2\rangle_v$ as a function of the external field, and we have applied the method to bulk samples of nanocrystalline electrodeposited Ni and Co and coarse-grained polycrystalline cold-worked Ni. The root-mean-square magnetostatic stray field, which is inherent to a particular magnetic microstructure, shows a pronounced field dependence, with values ranging from about 5 to 50 mT. Even at applied fields as large as 1.7 T, the quantity $\mu_0\langle|\mathbf{H}_d^b|^2\rangle_v^{1/2}$ of nanocrystalline Co is still 24 mT, which suggests that contributions to the total magnetostatic field originating from the bulk are significant in nanocrystalline ferromagnets; therefore, $\langle|\mathbf{H}_d^b|^2\rangle_v$ cannot be ignored in the interpretation of *e.g.* measurements of magnetization or spin-wave resonance. A comparison of $\langle|\mathbf{H}_d^b|^2\rangle_v$ with the volume-averaged mean-square anisotropy field reveals that both quantities are of comparable magnitude.

PACS. 61.12.Ex Neutron scattering techniques (including small-angle scattering) – 75.30.Gw Magnetic anisotropy – 75.50.Tt Fine-particle systems; nanocrystalline materials – 75.75+a Magnetic properties of nanostructures – 81.07.-b Nanoscale materials and structures: fabrication and characterization

1 Introduction

When a magnetic field $\mathbf{H}_a$ is applied to a ferromagnetic body, the magnetic moments inside the body begin to align along $\mathbf{H}_a$ and eventually, when the magnitude of $\mathbf{H}_a$ is large enough, all moments become aligned with the external field. However, several forces can give rise to torques on the magnetic moments that prevent them from reaching a state of perfect alignment. The most obvious force results from the combined effect of magnetocrystalline and magnetoelastic anisotropy. Additionally, magnetostatic stray fields can exert a torque on the magnetization $\mathbf{M}$ whenever divergences of $\mathbf{M}$ arise within the volume or at the outer surface of the ferromagnet. There are many instances where deviations from the perfectly aligned state of magnetic moments are of importance: historically, the most prominent example is the magnetization profile across a domain wall [1], but phenomena such as domain nucleation (see, *e.g.*, Ref. [2] and references therein), the effect of lattice defects on the approach to magnetic saturation [3–9], spin waves [10,11], the so-called "magnetization ripple" in thin films [12–15] and the magnetic properties of amorphous ferromagnets [16–18] remain the subject of contemporary research. Brown's equations of micromagnetics [19–21], which are non-linear partial integro-differential equations with complex boundary conditions, are used to describe the magnetic microstructure, *i.e.*, the spatial variation of the spin orientation on the scale of roughly $1 - 1000$ nm [22], in most of those investigations. Rigorous closed-form solutions to these equations are known for relatively few cases such as the nucleation problem [2]. Due to the complicated nature of Brown's equations, it is often necessary to make simplifying assumptions; among these are *e.g.* the disregard of magnetoelastic anisotropy, the linearization of the equations in the regime near magnetic saturation, and the neglect of the magnetostatic stray field that results from $\nabla \cdot \mathbf{M} \neq 0$ from within the bulk. In this study, we are concerned with the latter quantity, and we investigate the question how strong the magnetostatic dipole-dipole interaction field (due to $\nabla \cdot \mathbf{M} \neq 0$)

[a] e-mail: anmi@nano.uni.saarland.de

actually is in real specimens. To that end, we provide a theoretical treatment that enables computation of a lower bound for the magnetostatic stray field by combining the high-field solution of the basic equations of micromagnetics with the results of field-dependent magnetic small-angle neutron scattering (SANS) measurements. In particular, we investigate the strength and magnetic-field dependence of the volume-averaged mean-square magnetostatic stray field, and we scrutinize how it compares in magnitude to the perturbing field that arises from the magnetic anisotropy.

Nanocrystalline (nc) and microcrystalline cold-worked materials are particularly suited to such a study, since fluctuations of the magnetization present in these materials evolve on a length scale that can be probed by SANS, a technique having a spatial resolution of typically 1–500 nm. For instance, single-component, single-phase nc ferromagnets constitute dense arrangements of polyhedral grains with an average crystallite size D of typically 10 nm. Owing to the reduced grain size, the direction and/or strength of the magnetic anisotropy field changes randomly on a length scale of the order of D, thus giving rise to a static magnetic microstructure that is highly nonuniform on a nanometer scale. As a result of this nonuniformity, the *static* magnetic microstructure in nc magnets gives rise to a strong *elastic* magnetic neutron scattering signal at small scattering angles. In the light of the recent availability of high-purity, porosity-free electrodeposited nc soft magnets [23], characterized by a favorably high ratio of interesting *magnetic* scattering to *nuclear* background, nc magnets seem especially attractive for studies by magnetic SANS.

In fact, with such samples it has become possible to combine predictions for the magnetization distribution $\mathbf{M}(\mathbf{x})$ from micromagnetics theory [19–21] with experimental magnetic SANS in a straightforward way, similar to what is established in the fields of ferromagnetic and spin-wave resonance. The approach of combining micromagnetics computations with SANS was previously used to investigate the arrangement of dislocations in plastically deformed Fe single crystals [24], and it has been applied to study the magnetic microstructure of nc electrodeposited Ni and Co [25–29].

The paper is organized as follows: Section 2 describes the basic formalism used to obtain the volumetric mean-square magnetostatic stray field. Section 3 presents the micromagnetics model. In Section 4, we discuss the SANS cross-section of nc ferromagnets near saturation, and we establish the connection between micromagnetics and experimental SANS data to yield the volume-averaged magnetostatic stray field. Finally, Section 5 presents and discusses the results.

2 Magnetostatics

According to the well-known expression for the magnetostatic potential of a distribution of magnetic volume and surface charges [30], we can separate the total demagnetizing field $\mathbf{H}_d(\mathbf{x})$ into a contribution $\mathbf{H}_d^b(\mathbf{x})$ due to $\nabla\cdot\mathbf{M} \neq 0$ from within the volume of the sample and into a contribution $\mathbf{H}_d^s$ originating from the free magnetic poles at the macroscopic sample surface, *i.e.*, $\mathbf{H}_d = \mathbf{H}_d^b + \mathbf{H}_d^s$. At high applied fields H_a, when the magnetization $\mathbf{M}$ is only slightly misaligned from the direction of $\mathbf{H}_a$ – the situation that is considered throughout this paper – the vector $\mathbf{H}_d^s$ can (for a body of ellipsoidal shape) be assumed to be independent of position $\mathbf{x}$ within the material, and $\mathbf{H}_d^s$ is therefore approximated by the uniform field $\mathbf{H}_d^s = -N_d\,\langle\mathbf{M}\rangle$, where N_d denotes the demagnetizing factor that depends on the sample shape, and $\langle\mathbf{M}\rangle$ is the macroscopic mean magnetization, which is directed along $\mathbf{H}_a$. The magnitude of $\langle\mathbf{M}\rangle$ is $|\langle\mathbf{M}\rangle| = M_s\,|\langle\cos\delta\rangle|$, where M_s denotes the magnitude of $\mathbf{M}$, and δ is the local angle of misalignment of $\mathbf{M}$ relative to $\mathbf{H}_a$. In the small-misalignment regime $\delta \ll 1$, and $H_d^s \cong -N_d\,M_s$.

The contribution of the bulk to $\mathbf{H}_d$ is obtained by solving the basic equations of magnetostatics inside the ferromagnetic body [31],

$$\nabla\cdot\mathbf{M}(\mathbf{x}) = -\nabla\cdot\mathbf{H}_d^b(\mathbf{x}) \quad \text{with} \quad \nabla\times\mathbf{H}_d^b(\mathbf{x}) = 0\ . \tag{1}$$

Since in our linear micromagnetics theory (see Sect. 3 below) the sample is treated as infinitely large, it proves to be convenient to express the magnetization and the fields in terms of their Fourier transforms. By introducing $\mathbf{m}(\mathbf{q})$ as the Fourier coefficient of $\mathbf{M}_p(\mathbf{x})/M_s$, which represents the reduced transversal fluctuation of $\mathbf{M}(\mathbf{x})$ from its position-independent average $\langle\mathbf{M}\rangle$ (compare Fig. 1a),

$$\frac{\mathbf{M}_p(\mathbf{x})}{M_s} = \frac{\mathbf{M}(\mathbf{x}) - \langle\mathbf{M}\rangle}{M_s} = \frac{1}{(2\pi)^{3/2}}\int \mathbf{m}(\mathbf{q})\,\exp(\mathrm{i}\,\mathbf{q}\cdot\mathbf{x})\,\mathrm{d}^3q\ , \tag{2}$$

and by writing $\mathbf{H}_d^b(\mathbf{x})$ as a Fourier integral with corresponding Fourier coefficient $\mathbf{h}_d^b(\mathbf{q})$,

$$\mathbf{H}_d^b(\mathbf{x}) = \frac{1}{(2\pi)^{3/2}}\int \mathbf{h}_d^b(\mathbf{q})\,\exp(\mathrm{i}\,\mathbf{q}\cdot\mathbf{x})\,\mathrm{d}^3q\ , \tag{3}$$

we find the following solution to equation (1) [5,10]:

$$\mathbf{H}_d^b(\mathbf{x}) = -\frac{M_s}{(2\pi)^{3/2}}\int \frac{[\mathbf{m}(\mathbf{q})\cdot\mathbf{q}]\,\mathbf{q}}{q^2}\,\exp(\mathrm{i}\,\mathbf{q}\cdot\mathbf{x})\,\mathrm{d}^3q\ , \tag{4}$$

where $\mathbf{q}$ denotes a wave vector with modulus q. By comparison of equations (3, 4), we can identify the Fourier coefficient of $\mathbf{H}_d^b(\mathbf{x})$ as $\mathbf{h}_d^b(\mathbf{q}) = -M_s\,q^{-2}\,[\mathbf{m}(\mathbf{q})\cdot\mathbf{q}]\,\mathbf{q}$.

The volume-averaged mean-square magnetostatic stray field $\langle|\mathbf{H}_d^b|^2\rangle_v$ is defined by

$$\langle|\mathbf{H}_d^b|^2\rangle_v := \frac{1}{V}\int\limits_V |\mathbf{H}_d^b(\mathbf{x})|^2\,\mathrm{d}^3x\ , \tag{5}$$

where V is the sample volume. By use of the following property of Fourier integrals [32],

$$\int |\mathbf{H}_d^b(\mathbf{x})|^2\,d^3x = \int |\mathbf{h}_d^b(\mathbf{q})|^2\,\mathrm{d}^3q\ , \tag{6}$$

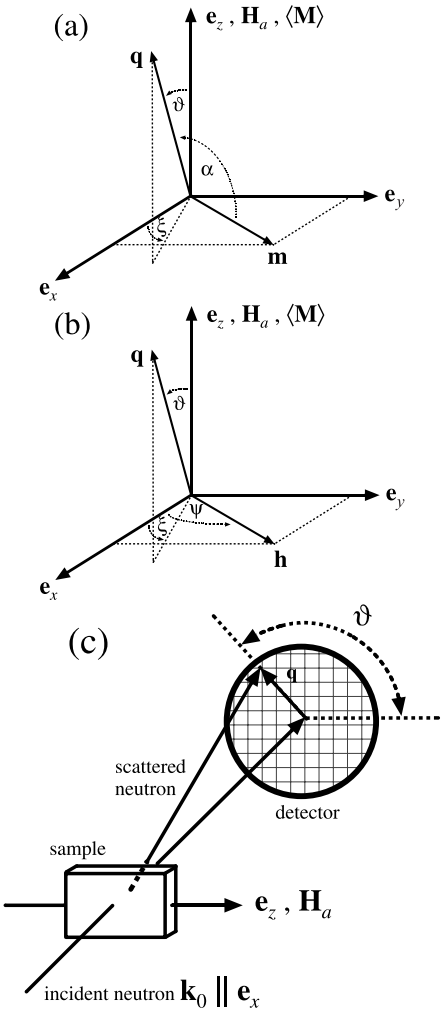

Fig. 1. (a) and (b) Sketches explaining the meaning of the angles α, ϑ, ξ and ψ. In the small-misalignment approximation, the spatial variation of $\mathbf{M}_p(\mathbf{x})$ and of $\mathbf{m}(\mathbf{q})$ is confined to the plane perpendicular to the applied magnetic field $\mathbf{H}_a$. The orientation of the wave vector $\mathbf{q}$ is specified by the angles ϑ and ξ. The anisotropy field $\mathbf{H}_p(\mathbf{x})$ and its Fourier coefficient $\mathbf{h}(\mathbf{q})$ vary in the x-y-plane. The unit vectors along the Cartesian coordinate axes are denoted by $\mathbf{e}_x$, $\mathbf{e}_y$ and $\mathbf{e}_z$. (c) Scattering geometry used in the SANS experiments. The scattering vector $\mathbf{q}$ lies in the plane perpendicular to the incoming neutron wave vector $\mathbf{k}_0$ ($\xi = \pi/2$).

we can rewrite equation (5) as

$$\langle|\mathbf{H}_d^b|^2\rangle_v = \frac{M_s^2}{V}\int |\mathbf{m}(\mathbf{q})|^2 \cos^2\alpha \, \mathrm{d}^3q \ , \qquad (7)$$

where α is the angle between $\mathbf{m}$ and $\mathbf{q}$. Obviously, for a fully saturated sample $\mathbf{M}_p(\mathbf{x}) = 0$ and, correspondingly, $\langle|\mathbf{H}_d^b|^2\rangle_v \equiv 0$.

By inspection of equation (7) we see that the magnetostatic field arises from those Fourier components of the magnetization with $\mathbf{m}$ parallel to $\mathbf{q}$. The magnetostatic field is associated with a self energy proportional to $\int_{\text{space}} |\mathbf{H}_d^b|^2 \, \mathrm{d}^3x$ [33], and, as a consequence of the pole avoidance principle, the equilibrium configuration of the spin system will exhibit a tendency to minimize fluctuations with $\mathbf{m} \parallel \mathbf{q}$. In other words, the effect of the magnetostatic interaction on the magnetic microstructure is to suppress selectively those Fourier components of $\mathbf{M}$ for which $\mathbf{m} \parallel \mathbf{q}$. By neglecting the magnetostatic field, one will therefore in general overestimate the mean-square misalignment angle and underestimate the net magnetization.

Equation (7) represents a central result, since it relates $\langle|\mathbf{H}_d^b|^2\rangle_v$ to the Fourier coefficient $\mathbf{m}(\mathbf{q})$ of the transversal component $\mathbf{M}_p(\mathbf{x})$ of the magnetization and, as shown below, the function $|\mathbf{m}(\mathbf{q})|^2 \cos^2\alpha$ can be related to data obtained from magnetic-field-dependent SANS experiments. However, with regard to experiment, it is important to note that the macroscopic differential *spin-misalignment* scattering cross-section $\mathrm{d}\Sigma_{\text{mag}}/\mathrm{d}\Omega$, which is measured by SANS near saturation, is proportional to the product $|\mathbf{m}(\mathbf{q})|^2 \sin^2\alpha$ [26,28,29]. Consequently, equation (7) cannot be evaluated directly in terms of the measured magnetic SANS cross-section. Rather, the computation of $\langle|\mathbf{H}_d^b|^2\rangle_v$ relies upon an expression for $\mathbf{m}(\mathbf{q})$ derived from theory.

3 Micromagnetics

It is straightforward to derive an equation for $\mathbf{m}(\mathbf{q})$ by making use of the theory of micromagnetics [19–21], which permits computing the magnetization vector field as a function of position. The balance-of-torques equation in static micromagnetism reads [19–21]

$$\left(\frac{2A}{\mu_0 M_s^2}\{\nabla^2 M_x\,, \nabla^2 M_y\,, \nabla^2 M_z\} + \mathbf{H}(\mathbf{x}) + \mathbf{H}_p(\mathbf{x})\right) \times \mathbf{M}(\mathbf{x}) = 0 \ , \qquad (8)$$

where A is the exchange-stiffness constant, μ_0 the permeability of free space, M_x, M_y and M_z denote the Cartesian components of the magnetization vector $\mathbf{M}(\mathbf{x})$, and $\mathbf{H}(\mathbf{x}) = \mathbf{H}_a + \mathbf{H}_d^b(\mathbf{x}) - N_d\langle\mathbf{M}\rangle$ represents the magnetic field, with $\mathbf{H}_a$ the applied magnetic field. $\mathbf{H}_p(\mathbf{x}) = -\mu_0^{-1}\{\partial\omega_a/\partial M_x, \partial\omega_a/\partial M_y, \partial\omega_a/\partial M_z\}$ is the anisotropy field, the derivative of the anisotropy-energy density ω_a with respect to the components of $\mathbf{M}$, which are subject to the condition $|\mathbf{M}| = M_s$. Generally, ω_a is a function of the position $\mathbf{x}$ and of powers of the components of $\mathbf{M}$, *i.e.*, $\omega_a = \omega_a(\mathbf{x}, \mathbf{M}(\mathbf{x}, \mathbf{H}_a))$. In the small-misalignment approximation, changes in ω_a due to a reorientation of $\mathbf{M}$ are small, and, therefore, ω_a can be assumed to depend only linearly on the components of $\mathbf{M}$ [3]. As a consequence, the resulting anisotropy field $\mathbf{H}_p$ is constant with respect to $\mathbf{M}$ and therefore does not depend on $\mathbf{H}_a$, implying that $\mathbf{H}_p = \mathbf{H}_p(\mathbf{x})$. Equation (8) states that at static equilibrium the torque on each magnetic moment arising from the combined effects of (i) the exchange interaction, (ii) the magnetic field and (iii) the anisotropy field vanishes, resulting in a magnetic microstructure characterized by an alignment of the magnetization $\mathbf{M}(\mathbf{x})$

parallel to the vector given in the parentheses of equation (8). Furthermore, the boundary conditions of equation (8) on the external sample surface can be ignored, since the specimen is assumed to be infinitely extended. According to Brown [3,34], such a supposition is justified whenever the sample dimensions are large compared to the static ferromagnetic correlation length l_C. Our recent SANS measurements on nc Ni and Co samples [35,36] indicate that l_C varies between about 10 nm (at high applied fields) and 100 nm (at small applied fields) – a length scale that is small compared to a typical scattering volume of $10 \times 10 \times 0.5\,\mathrm{mm}$.

Solutions to equation (8) have been derived in various contexts (see, *e.g.*, Refs. [19–21] and references therein). The relevant solution of equation (8) in the limit of small misalignment can formally be expressed in terms of the Fourier coefficient $\mathbf{m}(\mathbf{q})$ of the reduced transversal magnetization $\mathbf{M}_p(\mathbf{x})/M_s$ defined by equation (2) [29]. By assuming $\mathbf{H}_a$ (and, therefore, $\langle\mathbf{M}\rangle$) directed along the z-axis and for a general orientation of the wave vector $\mathbf{q} = \{q_x, q_y, q_z\}$, we obtain the following expressions for the Cartesian components of $\mathbf{m}(\mathbf{q})$:

$$
\begin{aligned}
m_x(\mathbf{q}) &= \frac{h_x(\mathbf{q})\left(H_{\mathrm{eff}} + M_s\,\frac{q_y^2}{q^2}\right) - h_y(\mathbf{q})\,M_s\,\frac{q_x\,q_y}{q^2}}{H_{\mathrm{eff}}\left(H_{\mathrm{eff}} + M_s\,\frac{q_x^2+q_y^2}{q^2}\right)}\,,\\
m_y(\mathbf{q}) &= \frac{h_y(\mathbf{q})\left(H_{\mathrm{eff}} + M_s\,\frac{q_x^2}{q^2}\right) - h_x(\mathbf{q})\,M_s\,\frac{q_x\,q_y}{q^2}}{H_{\mathrm{eff}}\left(H_{\mathrm{eff}} + M_s\,\frac{q_x^2+q_y^2}{q^2}\right)}\,,\\
m_z(\mathbf{q}) &= 0\,,
\end{aligned}
\tag{9}
$$

where terms of higher than linear order in $\mathbf{M}_p(\mathbf{x})$ have been neglected.

The functions $h_x(\mathbf{q})$ and $h_y(\mathbf{q})$ in equation (9) represent the components of the Fourier coefficient $\mathbf{h}(\mathbf{q})$ of the anisotropy field $\mathbf{H}_p(\mathbf{x})$,

$$
\mathbf{H}_p(\mathbf{x}) = \frac{1}{(2\pi)^{3/2}}\int \mathbf{h}(\mathbf{q})\,\exp(\mathrm{i}\,\mathbf{q}\cdot\mathbf{x})\,\mathrm{d}^3q\,, \tag{10}
$$

and the effective magnetic field,

$$
H_{\mathrm{eff}}(q, H_i) = H_i\left(1 + l_H^2\,q^2\right)\,, \tag{11}
$$

depends on q and on the magnitude of the internal field $H_i = H_a - N_d\,M_s$. The quantity $l_H = [2A/(\mu_0\,M_s\,H_i)]^{1/2}$ represents the exchange length of the internal field, which is characteristic of the length scale over which perturbations in the spin structure decay [26]. Note that within the small-misalignment approximation, *i.e.*, $|\mathbf{M}_p/M_s| \ll 1$, the variation of $\mathbf{M}_p(\mathbf{x})$ and of $\mathbf{m}(\mathbf{q})$ is confined to the plane perpendicular to $\mathbf{H}_a$ (see Fig. 1a). By following the arguments on page 7 of reference [19], it is seen that the vectors $\mathbf{H}_p(\mathbf{x})$ and $\mathbf{h}(\mathbf{q})$ also vary exclusively in the x-y-plane (see Fig. 1b). No assumption about the particular form of the magnetic anisotropy (magnetocrystalline and/or magnetoelastic) was made in deriving equation (9). It is also worth noting that the SANS measurements are performed with the incoming neutron wave vector $\mathbf{k}_0 \parallel \mathbf{e}_x$ oriented perpendicular to the applied magnetic field $\mathbf{H}_a$, implying therefore that the scattering vector $\mathbf{q}$ varies exlusively in the y-z-plane (compare Fig. 1c).[1] In this scattering geometry, only those Fourier components of the magnetization with $q_x = 0$ are probed. Nevertheless, since the results for $\langle|\mathbf{H}_d^b|^2\rangle_v$ and $\mathbf{m}(\mathbf{q})$, equations (7, 9), do not care for a particular scattering geometry, the most general representation for the vector $\mathbf{q}$ with $q_x \neq 0$ has to be used in the further calculation of $\langle|\mathbf{H}_d^b|^2\rangle_v$ (see below).

Since the central goal of this study is the computation of $\langle|\mathbf{H}_d^b|^2\rangle_v$ as given by equation (7), it is necessary to determine $|\mathbf{m}(\mathbf{q})|^2\cos^2\alpha$. This is achieved by specifying the orientation of $\mathbf{h}(\mathbf{q})$ in the x-y-plane by the angle ψ, *i.e.*, $\mathbf{h}(\mathbf{q}) = h(\mathbf{q})\,\{\cos\psi, \sin\psi, 0\}$ (compare Fig. 1b), and by expressing the factor $\cos^2\alpha$ as $\cos^2\alpha = [\mathbf{q}/q\cdot\mathbf{m}/m]^2$, where $\mathbf{q} = q\,\{\sin\vartheta\cos\xi, \sin\vartheta\sin\xi, \cos\vartheta\}$ (compare Fig. 1a). Finally, the resulting expression for $\langle|\mathbf{H}_d^b|^2\rangle_v$ is

$$
\langle|\mathbf{H}_d^b|^2\rangle_v = \frac{M_s^2}{V}\int \frac{h^2(\mathbf{q})\,\sin^2\vartheta\,\cos^2(\psi-\xi)}{\left(H_{\mathrm{eff}} + M_s\sin^2\vartheta\right)^2}\,\mathrm{d}^3q\,. \tag{12}
$$

In Section 4, we will see that the unknown function $h^2(\mathbf{q})$ in equation (12) can be related to an experimentally measurable quantity.

4 Small-angle neutron scattering as a probe for magnetic volume charges

The magnetic SANS formalism combined with micromagnetics theory has been successfully applied to study the magnetic microstructure of nc Ni and Co; in particular, information on the value of the exchange-stiffness constant and the magnitude and spatial variation of the magnetic anisotropy field were obtained by this method [26–29]. In fact, we have recently shown that, in the limit of near saturation, the total nuclear and magnetic SANS cross-section $\mathrm{d}\Sigma/\mathrm{d}\Omega$ of ferromagnets, such as nc or cold-worked materials, characterized by a highly nonuniform anisotropy-field microstructure can be written as

$$
\frac{\mathrm{d}\Sigma}{\mathrm{d}\Omega}(q, H_i) = \frac{\mathrm{d}\Sigma_{\mathrm{res}}}{\mathrm{d}\Omega}(q) + S_H(q)\,R(q, H_i)\,. \tag{13}
$$

Here, $d\Sigma_{\mathrm{res}}/d\Omega$ is a combined nuclear and magnetic residual scattering cross-section that takes into account SANS caused by nonuniformities in atomic density and/or composition of the material, such as pores. In the limit of small misalignment, $\mathrm{d}\Sigma_{\mathrm{res}}/\mathrm{d}\Omega$ is independent of H_i [29]. The term $S_H(q)\,R(q, H_i)$ denotes the magnetic-field-dependent, pure micromagnetic spin-misalignment scattering cross-section, which is written as the product of

[1] In order not to complicate the discussion, we denote with $\mathbf{q}$ the wave vector as well as the scattering vector.

the *anisotropy-field scattering function* $S_H(q)$ and the *micromagnetic response function for SANS* $R(q, H_i)$. The product $S_H(q)\,R(q, H_i)$ describes the magnetic SANS from small transversal magnetization components $\mathbf{M}_p(\mathbf{x})$, aligned perpendicular to the applied magnetic field, that have been discussed in the previous sections. Both quantities, $\frac{\mathrm{d}\Sigma_{\mathrm{res}}}{\mathrm{d}\Omega}(q)$ and $S_H(q)$, are *a priori* unknown functions of q that can be directly determined from experimental SANS data [28,29].

In order to elucidate the magnitude and field dependence of $\langle|\mathbf{H}_d^b|^2\rangle_v$, the function $S_H(q)$ is of special interest since, in the approach to magnetic saturation, S_H is proportional to the square magnitude of the Fourier coefficient $\mathbf{h}(\mathbf{q})$ of the anisotropy field, $\mathbf{H}_p(\mathbf{x})$ being the relevant quantity determining $\langle|\mathbf{H}_d^b|^2\rangle_v$ (compare Eqs. (10) and (12)). As shown in references [26,28,29],

$$S_H(q) = \frac{8\pi^3}{V}\, b_{\mathrm{mag}}^2\, \rho_a^2\, M_s^{-2}\, h^2(q)\ , \tag{14}$$

where b_{mag} denotes the atomic magnetic scattering length, and ρ_a is the atomic density. $S_H(q)$ carries information about the magnitude and spatial variation of the anisotropy field and, therefore, reflects microstructural details of a material, such as grain size, microstrain or lattice defects. The derivation of equation (14) assumed that S_H does not depend on the orientation of the scattering vector $\mathbf{q}$; therefore, equation (14) strictly applies only to statistically isotropic microstructures.

The central result of this paper is obtained by inserting the solution for $h^2(q)$ of equation (14) into equation (12). Averaging over the orientations of the anisotropy field in the plane perpendicular to $\mathbf{H}_a$, $(2\pi)^{-1}\int_0^{2\pi}\langle|\mathbf{H}_d^b|^2\rangle_v\,\mathrm{d}\psi$, and performing the integration of equation (12) with respect to the angles ϑ and ξ ($d^3q = q^2\sin\vartheta\,\mathrm{d}\vartheta\,\mathrm{d}\xi\,\mathrm{d}q$) yields the final expression for the volume-averaged mean-square magnetostatic stray field $\langle|\mathbf{H}_d^b|^2\rangle_v$:

$$\langle|\mathbf{H}_d^b|^2\rangle_v = \frac{M_s^2}{8\pi^2\, b_{\mathrm{mag}}^2\, \rho_a^2}\int_0^\infty S_H(q)\ q^2\, p^2 \times\left(\frac{(1+2p)\ln(\sqrt{p}+\sqrt{1+p}\,) - \sqrt{p+p^2}}{(p+p^2)^{3/2}}\right)\mathrm{d}q\,, \tag{15}$$

with the dimensionless parameter $p = M_s/H_{\mathrm{eff}}(q, H_i)$.

5 Results and discussion

As motivated in the introduction, we measured the SANS signal of nc electrodeposited Ni and Co samples and that of a cold-worked (cw) Ni sample as a function of applied magnetic field (and temperature). Previous studies performed on these materials found, firstly, that the nc samples are practically saturated at applied fields larger than about $0.1 - 0.2\,\mathrm{T}$ [29], suggesting that the small-misalignment approximation is valid at fields stronger than 0.2 T. Secondly, the measured values of the exchange-stiffness constants and saturation magnetizations are identical to the respective single-crystal values within an uncertainty of $\pm\,(1-2)\,\%$ [29]. This supports the assumption of materials homogeneity with respect to the exchange interaction and density. As a consequence, there is no need to consider discontinuities of the magnetization at internal defects like grain boundaries, and it is reasonable to neglect internal boundary conditions in the micromagnetics theory. All remaining experimental details, sample characterization, SANS data and the materials parameters used in the data analysis can be found in reference [29].

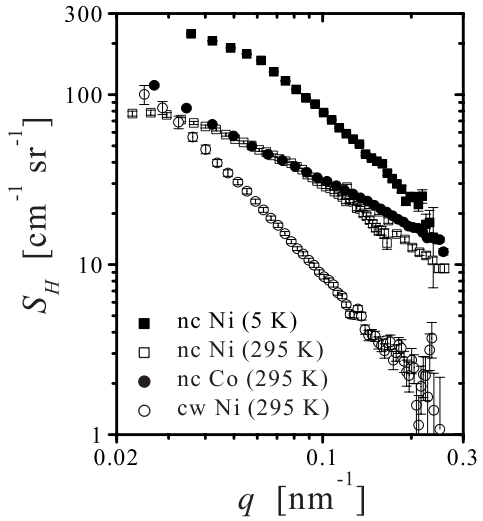

Fig. 2. Log-log plot of the anisotropy-field scattering function S_H of nc Ni, nc Co and coarse-grained polycrystalline cw Ni (see inset) as a function of the modulus q of the scattering vector [29].

Figure 2 shows the anisotropy-field scattering functions of nc Ni and Co and of coarse-grained polycrystalline cw Ni at several temperatures used in the computation of $\langle|\mathbf{H}_d^b|^2\rangle_v$ by numerical integration of equation (15) [29]. Due to the experimentally limited range of q-values, $0.025\,\mathrm{nm}^{-1} \lesssim q \lesssim 0.25\,\mathrm{nm}^{-1}$, the calculated values for $\langle|\mathbf{H}_d^b|^2\rangle_v$ represent lower bounds of this quantity. However, it was found that for all samples and at all fields the integrand in equation (15) showed signs of convergence at both ends of the integration interval (see Fig. 3), suggesting that, given the above q-range, the main contributions to $\langle|\mathbf{H}_d^b|^2\rangle_v$ originate from real-space magnetization fluctuations with a length scale $25\,\mathrm{nm} \lesssim 2\pi/q \lesssim 250\,\mathrm{nm}$. Magnetization inhomogeneities on a larger scale, for instance on the domain-size level, cannot be resolved with conventional SANS. By utilizing other techniques, like ultra small-angle neutron scattering (USANS), it should in principle be possible to reach q-values as small as $0.0005\,\mathrm{nm}^{-1}$ [37], which would enable $\langle|\mathbf{H}_d^b|^2\rangle_v$ to be determined with higher accuracy. Similarly, a stronger applied magnetic field would increase the maximum q-value [29].

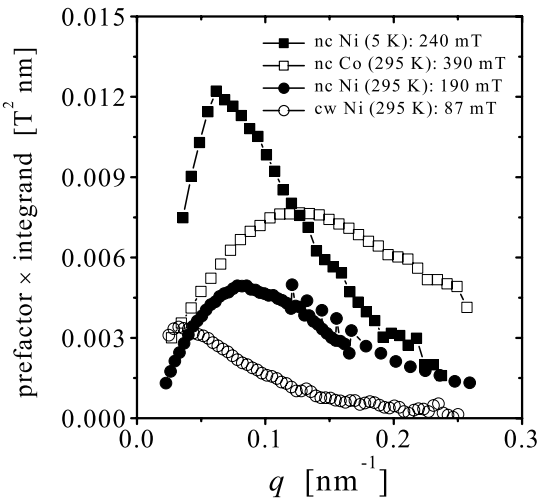

Fig. 3. The integrand of equation (15) multiplied by the constant prefactor at selected applied magnetic fields plotted as a function of q for nc Ni, nc Co and coarse-grained polycrystalline cw Ni (see inset). Lines are guide to the eye, and the respective values of the materials parameters were taken from reference [29].

Our results for $\langle|\mathbf{H}_d^b|^2\rangle_v$ are displayed in Figure 4, in which the root-mean-square magnetostatic field $\langle|\mathbf{H}_d^b|^2\rangle_v^{1/2}$ (in units of mT) is plotted as a function of the internal field H_i.

Note that the error bars shown in Figure 4 arise from the uncertainty in $S_H(q)$. Although the small-misalignment approximation is not satisfied at fields below $\approx (0.1-0.2)$ T, the experimental SANS cross-sections remain in good agreement with theoretical predictions down to the lowest fields investigated [29]. This indicates in particular that the linearized solution, equation (9), of the balance-of-torques equation continues to provide meaningful estimates for the Fourier components $\mathbf{m}(\mathbf{q})$ and, therefore, for the root-mean-square magnetostatic field. For this reason, we have included the estimated values of $\langle|\mathbf{H}_d^b|^2\rangle_v^{1/2}$ for the entire experimental range of applied fields in Figure 4, including values $\mu_0 H_i \lesssim (0.1-0.2)$ T.

For all samples investigated, the values of $\langle|\mathbf{H}_d^b|^2\rangle_v^{1/2}$ decrease when the internal field H_i is increased, since the contribution of the volume charges $\nabla\cdot\mathbf{M}$ to the total magnetostatic field is expected to decrease for an increasing degree of uniformity of the magnetic microstructure. The values of $\langle|\mathbf{H}_d^b|^2\rangle_v^{1/2}$ are largest for nc Co (Fig. 4a), since in Co stronger anisotropy fields (compared to Ni, see below) perturb the magnetization [29], resulting in a relatively less uniform magnetization distribution $\mathbf{M}(\mathbf{x})$ and, consequently, in larger values for $\langle|\mathbf{H}_d^b|^2\rangle_v^{1/2}$. A similar argument applies to explain the temperature dependence of $\langle|\mathbf{H}_d^b|^2\rangle_v^{1/2}$ observed for nc Ni (Figs. 4b and c). At $T = 5$ K stronger anisotropy fields result in a more inhomogeneous $\mathbf{M}(\mathbf{x})$ than at room temperature and, thus, in larger values for $\langle|\mathbf{H}_d^b|^2\rangle_v^{1/2}$ [29]. Coarse-grained polycrystalline cw Ni manifests the lowest values for $\langle|\mathbf{H}_d^b|^2\rangle_v^{1/2}$ (Fig. 4d). This is explained by the more homogeneous nature of the magnetic microstructure in microcrystalline Ni than in nc Ni over the length scale of $25-250$ nm estimated above. In contrast to nc Ni, where the magnetization is perturbed by inhomogeneous anisotropy fields on a nanometer scale (grain size: $D = 49$ nm [29]), fluctuations of $\mathbf{M}$ in coarse-grained Ni with a macroscopic grain size are expected to be present on a much larger length scale, giving rise to a magnetic SANS signal approaching the resolution limit of the technique. This is consistent with the overall lower values of S_H (compare Fig. 2) and the weaker magnetic SANS signal in this material (compare Fig. 5 in Ref. [29]).

The magnetic microstructure at equilibrium is governed by a balance of the various torque terms represented in equation (8). It is of interest to compare the action of the torque arising from the magnetostatic field to that caused by the main perturbing term, the field $\mathbf{H}_p(\mathbf{x})$. To this end, we compare the magnitude of the root-mean-square perturbing field to that of the root-mean-square magnetostatic field. By defining the volume-averaged mean-square anisotropy field as $\langle|\mathbf{H}_p|^2\rangle_v := V^{-1}\int_V |\mathbf{H}_p(\mathbf{x})|^2\,\mathrm{d}^3x$, assuming an isotropic microstructure and combining equations (6), (10) and (14), we arrive at an expression for $\langle|\mathbf{H}_p|^2\rangle_v$ that can be evaluated based on the experimental data for $S_H(q)$ [26]. Near saturation, the quantity

$$\langle|\mathbf{H}_p|^2\rangle_v = \frac{M_s^2}{2\pi^2\, b_{\mathrm{mag}}^2\, \rho_a^2}\int_0^\infty S_H(q)\; q^2\,\mathrm{d}q \qquad (16)$$

is a measure for the average perturbing field that acts as a torque on the magnetic moments and tries to deflect them from the perfectly aligned state.[2] Approximate lower bounds for $\langle|\mathbf{H}_p|^2\rangle_v^{1/2}$ were obtained by numerical integration of equation (16) using the experimental data for $S_H(q)$ shown in Figure 2. The results for $\langle|\mathbf{H}_p|^2\rangle_v^{1/2}$ are displayed in Figure 4 as horizontal lines, respectively [29]. In contrast to $\langle|\mathbf{H}_d^b|^2\rangle_v$, which depends on the internal field H_i through the effective magnetic field H_{eff} (compare Eq. (11)), $\langle|\mathbf{H}_p|^2\rangle_v$ does not depend on H_i, because the underlying anisotropy-energy density ω_a was assumed to depend linearly on the components of $\mathbf{M}$. A detailed discussion of the experimental values for $\langle|\mathbf{H}_p|^2\rangle_v^{1/2}$ and a comparison with the respective theoretical orientation-averaged anisotropy fields in single crystals can be found in reference [29].

[2] From its definition as the derivative of the anisotropy-energy density with respect to the components of $\mathbf{M}$, the perturbing field $\mathbf{H}_p$ has components normal to $\mathbf{M}$, which lead to a torque, and a component parallel to $\mathbf{M}$, which has no physical effect at all, since its cross product with $\mathbf{M}$ in equation (8) vanishes. Since SANS measures the Fourier components of the spin misalignment resulting from the perturbation by the nonuniform anisotropy, a SANS measurement provides information on the normal components of $\mathbf{H}_p$ exclusively. The result of equation (16) (horizontal lines in Fig. 4) refers to the expectation value of this quantity.

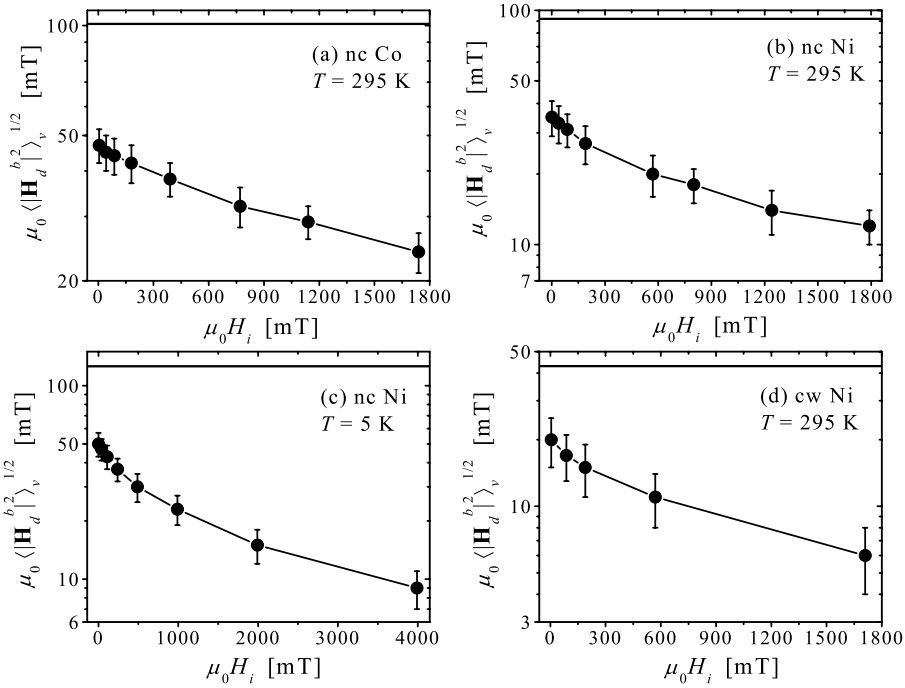

Fig. 4. Lower bounds for the volumetric root-mean-square magnetostatic stray field $\langle|\mathbf{H}_d^b|^2\rangle_v^{1/2}$, as determined from equation (15) for nc Co (a), nc Ni (b, c) and for coarse-grained polycrystalline cw Ni (d) as a function of the internal field H_i. Lines are guide to the eye. The horizontal line in each figure indicates the respective value of the volumetric root-mean-square anisotropy field $\langle|\mathbf{H}_p|^2\rangle_v^{1/2}$ (see text).

Comparing the results for $\langle|\mathbf{H}_p|^2\rangle_v^{1/2}$ and $\langle|\mathbf{H}_d^b|^2\rangle_v^{1/2}$, we see that the magnetostatic field takes on values of $30-50\,\%$ of the anisotropy field at the lowest applied fields. In other words, the magnetostatic field is comparable in magnitude to the anisotropy field. From the discussion in Section 2 it is obvious that the effects of the two fields are opposite: $\mathbf{H}_p$ is the origin of disorder in the spin system, whereas $\mathbf{H}_d^b$ suppresses the spin-misalignment fluctuations. Since the two terms are of comparable magnitude, neglecting $\mathbf{H}_d^b$ [38] can lead to substantial errors in micromagnetics computations of nc ferromagnets, even under near saturation conditions. It should also be noted that $\langle|\mathbf{H}_d^b|^2\rangle_v^{1/2}$ increases as the internal field H_i decreases, and that $\langle|\mathbf{H}_d^b|^2\rangle_v^{1/2}$ of the nc samples becomes larger than H_i for applied fields below typically $\mu_0 H_i \lesssim 40\,\mathrm{mT}$. This further supports our conclusion that the effect of $\mathbf{H}_d^b$ on the equilibrium configuration of the spin system is at least comparable to that of the remaining terms in the balance-of-torques equation, and that the neglect of $\mathbf{H}_d^b$ may have serious consequences for the predictions of micromagnetics models.

As a final remark, we suggest that our results might affect the analysis of magnetization and spin-wave resonance measurements. For instance, it is well known [39,40] that the nonuniform surface demagnetizing field of non-ellipsoidal bodies influences the spin-wave-excitation properties of a material, and, similarly, we would expect that the magnetostatic field $\mathbf{H}_d^b$ due to volume charges will also have a measurable effect on the excitation properties of spin waves in nc ferromagnets.

6 Summary and conclusions

In the near-saturation range, a combination of micromagnetics theory and SANS data provided the main result of this study, equation (15), from which a lower bound for the volume-averaged mean-square magnetostatic stray field $\langle|\mathbf{H}_d^b|^2\rangle_v$ arising from regions of $\nabla\cdot\mathbf{M}\neq 0$ in the bulk of a ferromagnet can be computed. $\langle|\mathbf{H}_d^b|^2\rangle_v$ was determined for nanocrystalline (nc) electrodeposited Ni and Co and for coarse-grained polycrystalline cold-worked (cw) Ni from experimental SANS data by determining the respective anisotropy-field scattering function $S_H(q)$, which contains information about the microstructure of the anisotropy field. The magnitude of $\mu_0\langle|\mathbf{H}_d^b|^2\rangle_v^{1/2}$ is largest in the nc samples, taking on values in the range $10-50\,\mathrm{mT}$, and smallest in microcrystalline Ni, for which it lies between 5 and 20 mT. Therefore, the reduction of relevant microstructural length scales down to the nanometer range is accompanied by a concomitant enhancement of the strength of the effect of volume charges. We suggest that $\langle|\mathbf{H}_d^b|^2\rangle_v$ will affect micromagnetic computations and magnetic measurements on nanostructured magnetic materials at *all* experimentally relevant fields.

The nanocrystalline samples were kindly provided by Prof. Uwe Erb from the University of Toronto. We thank Dr. Carl Krill for a critical reading of the manuscript and Dr. John Barker from NIST for help with the SANS experiments. This work has been supported by the Deutsche Forschungsgemeinschaft (Sonderforschungsbereich 277). A. Michels acknowledges financial support by the DAAD through a HSP-III scholarship.

References

1. L. Landau, E. Lifshitz, Phys. Z. Sowjetunion **8**, 153 (1935)
2. A. Aharoni, *Introduction to the Theory of Ferromagnetism*, 2nd edn. (Clarendon Press, Oxford, 1996), Chap. 9
3. W.F. Brown Jr., Phys. Rev. **58**, 736 (1940)
4. W.F. Brown Jr., Phys. Rev. **60**, 139 (1941)
5. T. Holstein, H. Primakoff, Phys. Rev. **59**, 388 (1941)
6. H. Kronmüller, in *Moderne Probleme der Metallphysik*, edited by A. Seeger (Springer-Verlag, Berlin, 1966), Vol. 2, pp. 24–156 (in German)
7. H. Kronmüller, J. Ulner, J. Magn. Magn. Mater. **6**, 52 (1977)
8. M. Fähnle, H. Kronmüller, J. Magn. Magn. Mater. **8**, 149 (1978)
9. H. Kronmüller, M. Fähnle, M. Domann, H. Grimm, R. Grimm, B. Gröger, J. Magn. Magn. Mater. **13**, 53 (1979)
10. C. Herring, C. Kittel, Phys. Rev. **81**, 869 (1951)
11. G. Bertotti, I.D. Mayergoyz, C. Serpico, Phys. Rev. Lett. **87**, 217203 (2001)
12. H. Hoffmann, J. Appl. Phys. **35**, 1790 (1964)
13. K.J. Harte, J. Appl. Phys. **39**, 1503 (1968)
14. W. Maass, U. Krey, H. Hoffmann, J. Magn. Magn. Mater. **53**, 330 (1986)
15. H. Hoffmann, Thin Solid Films **373**, 107 (2000)
16. E.M. Chudnovsky, R.A. Serota, Phys. Rev. B **26**, 2697 (1982)
17. E.M. Chudnovsky, R.A. Serota, J. Phys. C **16**, 4181 (1983)
18. E.M. Chudnovsky, W.M. Saslow, R.A. Serota, Phys. Rev. B **33**, 251 (1986)
19. W.F. Brown Jr., *Micromagnetics* (Interscience Publishers, New York, 1963)
20. S. Shtrikman, D. Treves, in *Magnetism III*, edited by G.T. Rado, H. Suhl (Academic Press, New York, 1963), Vol. 3, pp. 395–414
21. See chapters 7–11 in the book by Aharoni cited in reference [2]
22. A. Hubert, R. Schäfer, *Magnetic Domains* (Springer, Berlin, 1998), p. 10
23. R.T.C. Choo, J.M. Toguri, A.M. El-Sherik, U. Erb, J. Appl. Electrochem. **25**, 384 (1995)
24. G. Göltz, H. Kronmüller, A. Seeger, H. Scheuer, W. Schmatz, Philos. Mag. A **54**, 213 (1986)
25. J. Weissmüller, R.D. McMichael, J.G. Barker, H.J. Brown, U. Erb, R.D. Shull, Mater. Res. Soc. Symp. Proc. **457**, 231 (1997)
26. J. Weissmüller, R.D. McMichael, A. Michels, R.D. Shull, J. Res. Natl. Inst. Stand. Technol. **104**, 261 (1999), `http://www.nist.gov/jres`
27. A. Michels, J. Weissmüller, A. Wiedenmann, J.G. Barker, J. Appl. Phys. **87**, 5953 (2000)
28. A. Michels, J. Weissmüller, A. Wiedenmann, J.S. Pedersen, J.G. Barker, Philos. Mag. Lett. **80**, 785 (2000)
29. J. Weissmüller, A. Michels, J.G. Barker, A. Wiedenmann, U. Erb, R.D. Shull, Phys. Rev. B **63**, 214414 (2001)
30. See p. 125 in the book by Aharoni cited in reference [2]
31. See chapter 6 in the book by Aharoni cited in reference [2]
32. G. Arfken, *Mathematical Methods for Physicists*, 3rd edn. (Academic Press, San Diego, 1985), p. 812
33. See p. 146 in the book by Aharoni cited in reference [2]
34. See p. 63 in reference [19]
35. A. Michels, J. Weissmüller, U. Erb, J.G. Barker, Phys. Stat. Sol. (a) **189**, 509 (2002)
36. A. Michels and J. Weissmüller, unpublished (2002)
37. See `http://rrdjazz.nist.gov/instruments/usans/`
38. A. Aharoni, Physica B **306**, 1 (2001)
39. J.R. Eshbach, Phys. Rev. Lett. **8**, 357 (1962)
40. R.I. Joseph, E. Schlömann, J. Appl. Phys. **36**, 1579 (1965)